CYCLONE GLOBAL NAVIGATION SATELLITE SYSTEM (CYGNSS)

Algorithm Theoretical Basis Document Level 1A DDM Calibration	**UM Doc. No.**	**148-0136**
	SwRI Doc. No.	**N/A**
	Revision	**Rev 4**
	Date	**8 December 2023**
	Contract	**NNL13AQ00C**

Algorithm Theoretical Basis Documents (ATBDs) provide the physical and mathematical descriptions of the algorithms used in the generation of science data products. The ATBDs include a description of variance and uncertainty estimates and considerations of calibration and validation, exception control and diagnostics. Internal and external data flows are also described.

SPACE PHYSICS RESEARCH LABORATORY

SwRI®

NASA

CYCLONE GLOBAL NAVIGATION SATELLITE SYSTEM (CYGNSS)		
Algorithm Theoretical Basis Document Level 1A DDM Calibration	**UM Doc. No.**	**148-0136**
	SwRI Doc. No.	**N/A**
	Revision	**Rev 4**
	Date	**8 December 2023**
	Contract	**NNL13AQ00C**

Prepared by: Scott Gleason, Mohammad Al-Khaldi, Darren McKague. December, 2023

Approved by: Chris Ruf, CYGNSS Principal Investigator Date: 12/8/2023

Approved by: Anthony Russel, CYGNSS SOC Manager Date: 12/8/2023

Approved by: Darren McKague, CYGNSS UM Project Manager Date: 12/8/2023

REVISION NOTICE

Document Revision History		
Revision	**Date**	**Changes**
PRE-RELEASE DRAFT	17 June 2013	N/A
INITIAL RELEASE	14 January 2014	Add explicit algorithms for use of internal black body target and estimation of receiver noise temperature. Add detailed error analysis.
Rev 1	19 December 2014	Same basic approach but greater detail and examples provided of algorithm implementation.
Rev 2	20 August 2018	Inclusion of all modifications made to the Level 1A algorithms based on observed on-orbit performance between March 2017 and August 2018.
Rev 3	1 November 2023	Moved bin ratio correction section into L1a ATBD from L1b ATBD. Updated bin ratio correction algorithm.
Rev 4	8 December 2023	Added section summarizing changes by version.

Table of Contents

I. SUMMARY OF LEVEL 1 CHANGES PER VERSION 6
II. INSTRUMENT LEVEL 0 MEASUREMENTS 7
A. Level 0 Delay Doppler Map 7
B. Noise Power Expressions 7
C. Instrument Calibration Measurements 8
D. Instrument Noise Power Estimation Using Look Up Table 9
III. ROUTINE CALIBRATION OF SIGNAL POWER 9
A. Generating the Level 1a Data Product 10
B. Consideration of Time and Temperature Dependencies 10
C. Quality Control Flags 10
IV. ERROR ANALYSIS OF THE LEVEL 1A CALIBRATION ALGORITHM 11
V. CYGNSS LEVEL-1 BIN RATIO CORRECTIONS 12
A. CYGNSS Analog to Digital Convertor (ADC) Design 12
B. Uncorrected NBRCS Dependence on Bin Ratio 13
C. Bin Ratio Correction Design 13
D. NBRCS vs Bin Ratio Dependence After New Correction 15
E. Bin Ratio Based Corrections Application To Zenith Channel Observables 16

I. SUMMARY OF LEVEL 1 CHANGES PER VERSION

TABLE 1

SUMMARY OF LEVEL 1 CONFIGURATIONS PER MAJOR RELEASED VERSION

	V1.0	V2.1	V3.0	V3.1	V3.2
EIRP Calculation	Static	Static	Dynamic	Dynamic	Dynamic
Zenith/Specular Ratio Correction Version	N/A	N/A	v17	v19	v22
Thermal Oscillation	No	No	No	No	Yes
Black Body BR Correction	No	No	No	No	Yes
Zenith BR Correction	No	No	No	Yes, Signal Counts	Yes, Signal Counts
Nadir BR Correction	No	No	No	Yes, Noise Counts (CN)	Yes, Signal Counts (C-CN)
Nadir Antenna Pattern	v1	v6	v9	v17	v20

Table 1 summarizes the major changes and Science Operations Center Look-Up-Table (LUT) versions for each major CYGNSS Level 1 data product release from 2017 though 2023. Notes on each parameter are as follows,

a) EIRP Calculation. The initial calibration versions consisted of static LUTs to estimate the Effective Isotropic Radiated Power (EIRP) of the GPS transmitters. These initial estimates did not account for GPS “flex power” events which occurred periodically on certain GPS satellites (notably Block IIF, and others). An algorithm to dynamically estimate the transmitter EIRP was developed and put into place starting with v3.0 (See UM 148-0137 L1b document).

b) The ZSR Correction. This correction LUT serves to convert the EIRP power measured by the zenith antenna to the specular point direction based on the reflection geometry. As more data was gathered and the algorithm fine-tuned, improved versions were used in consecutive version releases.

c) The Thermal Oscillation Correction was first introduced in v3.2 and is described in what follows.

d) Initial Zenith and Nadir Bin Ratio (BR) corrections were first introduced in v3.1. This initial correction was based on scaled model corrections to both the zenith signal counts and nadir channel noise counts (See Section V.D). However, related degradations to the signal sensitivity to various geophysical properties of interest noted after release motivated a re-design of the BR correction strategy. The new strategy involved separate BR corrections to the a) black body counts and b) the signal counts on the nadir channels calculated as the total counts – noise counts.

e) The science antenna pattern versions went through several iterations and upgrades across the different versions. Notably, v6 in the v2.1 release includes an empirically based correction to the pattern. The v9 antenna pattern in v3.0 included model scaled corrections, which improved performance but were thought to result in unrealistically low antenna gain. The v17 antenna was based on a WW3 surface model but adjusted in magnitude to bring antenna gains closer to pre-launch levels. The v20 pattern in v3.2 was changed to use a reference of the mean gain across all patterns and was disconnected from the ocean model to provide more realistic gain levels while maintaining the optimized correction in pattern shape. The v3.2 patterns produce downstream NBRCS with no FM, starboard/port, or SV dependence with only minor shift (max .3 dB) from pre-launch chamber measurements.

II. INSTRUMENT LEVEL 0 MEASUREMENTS

This is a portion of the overall Level 1 Calibration Algorithm Theoretical Basis Document (ATBD) describing the Level 1a calibration and error analysis. Additional details on this algorithm together with the Level 1b calibration can be found in [1].

Individual bins of the DDM generated by the Delay Doppler Mapping Instrument (DDMI) are measured in raw, uncalibrated units referred to as "counts". These counts are linearly related to the total signal power processed by the DDMI. In addition to the ocean surface scattered Global Positioning System (GPS) signal, the total signal includes contributions from the thermal emission by the Earth and by the DDMI itself. The power in the total signal is the product of all the input signals, multiplied by the gain of the DDMI receiver. Level 1a calibration converts each bin in the DDM from raw counts to units of watts. A flowchart of the L1a calibration procedure is shown in Figure 1.

Calibration Intervals: The black body calibration was initially performed every 60 seconds for the first several years of the mission, but later changed to 600 seconds based on the analysis in [2] on-orbit for each nadir science antenna. The routine calibration is performed at 1Hz or 2Hz on all DDM's output by the DDMI depending on its output configuration (4 or 8 per second).

A. Level 0 Delay Doppler Map

The DDM values output from the CYGNSS science instrument will be sent to the CYGNSS spacecraft as arbitrary counts. The count values will be a result of the signal traveling through the various stages of the instrument, which will add a gain to the received power levels. The value of the pixels in the DDM in arbitrary counts can be linked to the arriving signal power in Watts such that,

$$C = G\left(P_a + P_r + P_g\right) \tag{1}$$

where,

C are the DDM values in counts output from the instrument at each delay/Doppler bin.
P_a is the thermal noise power received by the antenna in watts.
P_r is the thermal noise power generated by the instrument in watts.
P_g is the scattered signal power received by the instrument in watts.
G is the total instrument gain applied to the incoming signal and noise in counts per watt.

The terms, C and P_g are functions of delay and Doppler while P_a and P_r are assumed to be independent of the delay Doppler bin in the DDM. Every DDM includes a number of delay bins where signal power is not present and an individual DDM noise floor level can be estimated. These bins physically represent delays above the ocean surface. These delay and Doppler bins provide an estimate of the DDM noise power, expressed in counts as,

$$C_N = G(P_a + P_r) \tag{2}$$

Assuming P_a and P_r are independent of delay and Doppler, the DDM samples above the ocean surface can be used to estimate the noise only contribution to the raw counts expressed in Equation 1.

B. Noise Power Expressions

The input antenna noise can be generically expressed as,

$$P_a = kT_aB_w \tag{3}$$

where T_a is the top of the atmosphere brightness temperature integrated over the receive antenna pattern, k is Boltzmann's constant and $B_W = \frac{1}{T_i} = 1000$ Hz is the signal bandwidth. The bandwidth of the GPS signal at the antenna is determined by the coherent integration processing interval, which is T_i = 1 ms.

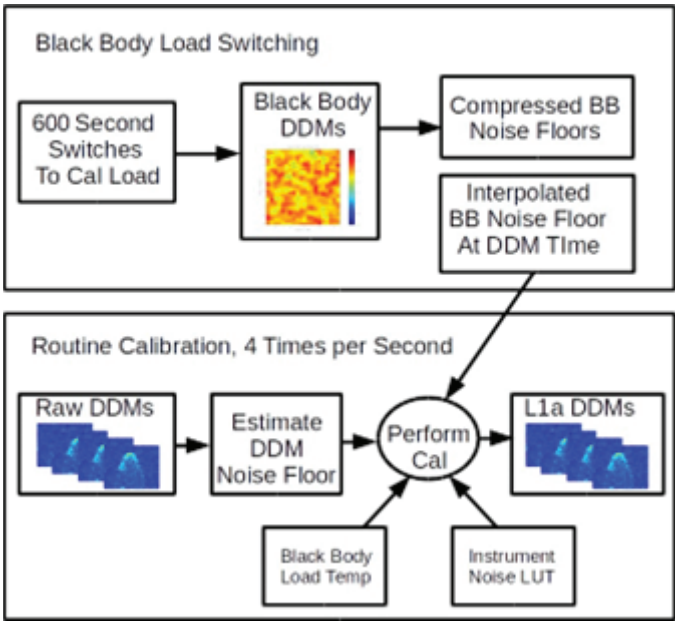

Fig. 1. Overview of CYGNSS Level 1a Calibration. The switches to the calibration load on each of the nadir antennas is performed every 60 seconds, initially and currently 600 seconds to obtain an estimate of the instrument only noise counts C_B. This in combination with the estimated DDM noise floor C_N, black body load physical temperature T_I and pre-launch characterized instrument noise power P_r are used to generate the calibrated L1a DDMs

When the instrument input is switched to the calibration load, the input antenna noise becomes,

$$P_B = kT_I B_W \tag{4}$$

where, P_B and T_I are the noise power and effective temperature of the instrument black body load source. The black body load resistor lies on thermal continuous LNA main board where temperature sensor is located, thus BB load temperature and LNA portion of the instrument are assumed to be nearly equivalent. T_I refers to the physical temperature of the Instrument LNA and black body load resistor in this analysis.

The instrument thermal noise power can be expressed as a function of the instrument noise figure,

$$P_r = kT_r B_W = k[(NF - 1)290]B_W \tag{5}$$

where, P_r and T_r are the instrument noise power and temperature. The receiver noise figure NF is directly related to the instrument noise temperature. The noise figure versus temperature profile was characterized pre-launch for all instrument LNAs, providing an accurate estimate of the instrument noise figure as a function of temperature, from which the instrument noise power can be calculated using Equation 5.

C. Instrument Calibration Measurements

The instrument noise power will be initially calculated using gain and noise figure temperature profiles generated prelaunch for both instrument LNAs on each satellite. Using these tables the instrument noise power can be estimated directly from the LNA temperature T_r and Equation 5.

Subsequently, the expression for the DDM noise counts when the instrument is switched to the black body calibration load can be calculated as,

$$C_B = G(P_B + P_r) \tag{6}$$

where P_B is the black body noise power and P_r is the instrument power. P_B can be calculated using Equation 4 and P_r is calculated using pre-launch look up tables and Equation 5.

D. Instrument Noise Power Estimation Using Look Up Table

It will be necessary to estimate the instrument noise power at every measurement due to LNA temperature fluctuations. This will be done using a look up table derived from measured characteristics of the LNA gain and noise figure as a function of temperature. Thermal testing of the LNA noise figure performance as a function of temperature for all 24 CYGNSS LNAs (one zenith and two nadir per spacecraft) was performed over several thermal cycles to generate a best linear fit function which is used to estimate the noise figure as a function of temperature on-orbit.

The mean standard deviation of the noise figure across the range of temperatures is 0.027 dB. The maximum slope is 0.0088 dB/DegC, which when multiplied by the temperature uncertainty results in an estimated error in the instrument noise figure of 0.018 dB due to temperature uncertainty. The total noise figure error is taken as the RSS of the standard deviation of the measurements and the temperature error, which is 0.032 dB.

The temperature of the LNA is read at 1 Hz and the value of the instrument noise figure is retrieved from a LUT generated from pre-launch testing. The LUT can then be updated on orbit using instrument noise floor estimates performed at sufficient intervals to track slow changes in the LNA performance. The instrument noise figure from the LUT is related to the instrument noise power using Equation 5.

The CYGNSS LNAs are proving to be remarkably stable, even after more than 6-years on orbit. Nonetheless, they are being closely monitored on a monthly basis for signs of aging and degradation. A number of techniques using the full set of existing on-orbit data are being explored to quantify the very small changes in the instrument noise figure as the instrument ages on-orbit and to update the instrument calibration LUTs accordingly if required. Notably, the instrument LNA LUTs were used to correct for an observed long duration temperature dependent oscillation that was impacting L1b parameters. This correction is described in detail in the CyGNSS L1B ATBD.

III. ROUTINE CALIBRATION OF SIGNAL POWER

The generic instrument DDM in counts is expressed in Equation 1, which includes the received signal power, P_g. These DDMs will be generated by the instrument at a 1 or 2 Hz rate and will be corrected by the estimated noise floor expressed in Equation 2 and calculated using noise only bins in the DDM, such that we are left with a signal only DDM,

$$C_g = C - C_N = GP_g \tag{7}$$

Subsequently the instrument gain at the collection time of the DDM can be calculated using the current estimate of the LNA physical temperature, T_I, from which we estimate the instrument noise power, P_r. This is achieved by re-arranging Equation 7 into an expression of the instrument gain, and setting this equal to the instrument gain expression obtained from the black body load calibration DDM from Equation 6,

$$G = \frac{C - C_N}{P_g} = \frac{C_B}{P_B + P_r} \tag{8}$$

where, C_B is the best estimate mean counts of the black body load DDM at the time of the measurement being calibrated. The black body load counts are linearly interpolated to the time of the measurement using black body DDMs before and after the DDM being calibrated.

P_B is the estimated black body load noise power estimated using the last LNA instrument thermistor temperature reading $T_I$near the load itself in the LNA, and Equation 4. Taken within a second of the DDM being calibrated.

P_r is the estimate of the instrument noise power, estimated from the noise figure vs physical temperature (T_I) look up table generated pre-launch for this specific LNA.

A. Generating the Level 1a Data Product

The routine calibration assumes that the Gain, G, antenna noise temperature T_a, and the instrument noise power P_r, remain constant over the combined collection interval for Equation 1 (DDM to be calibrated) and Equation 2 (Noise floor estimate for the DDM being calibrated). The black body noise counts used in Equation 6 is linearly interpolated from black body DDMs before and after the calibration DDM to the measurement time. By substituting Equation 7 into Equation 8 and solving for the signal power term, P_g we arrive at the final Level 1a calibration,

$$P_g = \frac{(C - C_N)(P_B + Pr)}{C_B} \tag{9}$$

Equation 9 is applied to all pixels of the compressed Level 0 DDMs (11 Doppler bins x 17 delay bins) for each instrument measurement channel. Related routine data processing has been updated for CYGNSS's v3.1 and v3.2 data releases. For a comprehensive overview, see Section IV.

B. Consideration of Time and Temperature Dependencies

All of the terms in Equation 9 are collected at slightly different times than the actual science measurements themselves, and during these time intervals it is possible that the noise temperatures can vary slightly from the measurement time. Each of the terms in the Level 1a calibration equation is addressed below with regard to this time difference,

1) The science measurement is made once per second per channel and provides the reference time for all of the other parameters.
2) C_N The noise measurements for each science DDM are made at delays above the ocean surface, which are only on the order of a handful of microseconds from the time of the science measurement.
3) P_B the blackbody target power is determined from a physical temperature sensor measured at 1 Hz and near enough in time that the physical temperature will not have changed significantly between the thermistor reading and the science measurement.
4) P_r the receiver noise power is derived from a pre-launch generated LUT and will be subject to change over the mission lifetime due to instrument aging effects. This will be corrected by periodically updating the calibration LUTs over the duration of the mission as described above. It is expected that the aging effects to occur on a very slow time scale, on the order of several months.
5) C_B the blackbody target measurement is made within 30 seconds of the science measurement and linearly interpolated to the measurement time using black body measurements before and after the DDM being calibrated. The analysis preformed in [2] demonstrated that a 600 second blackbody switching interval did not significantly degrade the calibration.

The LUTs used to estimate P_r will be updated on orbit as required. The dependence of P_r on temperature has been initially characterized in pre-launch environmental testing and the baseline flight lookup table was derived from those test data.

C. Quality Control Flags

The Level 1 data product will include a set of quality control flags designed to indicate to users potential problems with the data. Refer to the CYGNSS Level 1b ATBD for a complete list of quality flags [3].

IV. ERROR ANALYSIS OF THE LEVEL 1A CALIBRATION ALGORITHM

The Level 1a data product consists of observed signal power, P_g (in Watts) over a range of delay steps and Doppler frequencies. This error analysis concentrates on the uncertainties present in the CYGNSS Level 1a calibration algorithm. Each uncertainty in the Level 1a calibration algorithm will be considered as an independent uncorrelated error source. The method for this error analysis is based on that presented in Jansen et. al [4] for a microwave radiometer. The errors in the L1a calibration can be broken into two parts; the estimation of the instrument noise performed during the open ocean calibration sequence, P_r and the routine second by second calibration of the science DDM, P_g.

Equation 9 for the routine calculation of the calibrated signal power is repeated below,

$$P_g = \frac{(C - C_N)(P_B + Pr)}{C_B} \tag{10}$$

The total error in the estimate of the signal power, P_g, is the root sum square (RSS) of the individual errors contributed by the independent terms of Equation 10, expressed as,

$$\Delta P_g = \left[\sum_{i=1}^{5} E^2(p_i)\right]^{1/2} \tag{11}$$

where the partial derivatives of the individual errors terms can be expressed as,

$$E(p_i) = \left|\frac{\partial P_g}{\partial p_i}\right| \Delta p_i \tag{12}$$

The individual error quantities are defined as: $p_1 = C$, $p_2 = C_N$, $p_3 = P_B$, $p_4 = P_r$ and $p_5 = C_B$. The 1-sigma uncertainties in these quantities are expressed as Δp_i. Using Equation 10 and Equation 12 to evaluate the partial derivative error terms we obtain,

$$E(C) = \frac{P_B + P_r}{C_B} \Delta C \tag{13}$$

$$E(C_N) = \frac{P_B + P_r}{C_B} \Delta C_N \tag{14}$$

$$E(P_B) = \frac{C - C_N}{C_B} \Delta P_B \tag{15}$$

$$E(P_r) = \frac{C - C_N}{C_B} \Delta P_r \tag{16}$$

$$E(C_B) = \frac{(C - C_N)(P_B + P_r)}{C_B^2} \Delta C_B \tag{17}$$

The 1-sigma uncertainties in these quantities are expressed as Δp_i. The L1a 1-sigma uncertainties and the resulting partial derivative error terms are shown in Table 2.

TABLE 2

ESTIMATES LEVEL 1A 1-SIGMA UNCERTAINTIES, INDIVIDUAL ERROR CONTRIBUTIONS AND ROLLED UP L1A ERROR ESTIMATE

Error Term	Error Magnitude, dB	Comment
$E(C)$	0.10	Quantization and non-common mode interference
$E(C_N)$	0.14	DDM Noise Floor (45 row by 20 pixel average)
$E(P_B)$	2 deg C	Calibration Load Noise Power (from load temperature)
$E(P_r)$	0.14	Instrument Noise Power (from pre-launch LUT uncertainty)
$E(C_B)$	0.05	Calibration Load DDM Noise Counts
Total RSS L1a Error	0.13	From Partial Derivatives and MC Simulation
$E(C_N)$	0.14	DDM Noise Floor (45 row by 20 pixel average)

ΔC is the combination of the quantization error (negligible) and non-common mode contributions to the signal counts. The latter can include cross correlations with other GPS satellites which would not affect the signal and noise floors equally and cancel out in the L1a calculation made in Equation 10. Although it is not possible to accurately quantify exactly the error that may be introduced in the actual data, simulations showed that as a worse case, for certain PRN cross correlations, this error could be up to 0.1 dB.

1) ΔC_N is driven by the number of noise bins averaged during the routine calibration. This method has not changed from the analysis presented in [1]. However, the more conservative high wind speed value of 0.14 dB is used to better bound the error and to account for the possibility for mild RFI levels which would not be detected by the RFI detection algorithm.
2) ΔP_B is determined by the accuracy of the temperature sensor on the black body calibration load.
3) ΔP_r was calculated from the 1-sigma variation in the pre-launch raw measurements used to generate the instrument noise figure vs temperature look up table.
4) ΔC_B is estimated from the expected error after averaging a full black body calibration DDM (128 rows by 20 columns). Includes a small error component due to the propagation to the DDM measurement time between switches of the calibration load.

V. CYGNSS LEVEL-1 BIN RATIO CORRECTIONS

A. CYGNSS Analog to Digital Convertor (ADC) Design

A full explanation of the initial CYGNSS analog to digital sampling configuration and calibration corrections implemented in v3.1 can be found in [5].

The CYGNSS instrument input signal processing chain includes the following steps: After capturing the off-air signal by the receive antenna, the signal enters the low noise amplifier (LNA) and is processed through a cavity filter and initial fixed voltage gain stage. Following this initial amplification stage, the received signal travels to the instrument front end where additional down-conversion and filtering is applied. This includes added amplification by a commandable voltage gain which permits adjustment of the analog signal level into the ADC. It is noted, that numerous GPS receivers configure the front end into an Automatic Gain Control (AGC) mode in order to autonomously adjust this variable gain stage, thereby securing an ideal Normal sampling distribution. However, the need for knowledge of the precise input power level for a science observation prohibits this convenience on the CYGNSS instruments, and necessitates that the commandable gain stage remains at a constant commanded value for the CYGNSS receivers.

The need to manually command the front end gain settings, adds the requirement that the input signal levels be compatible with the 2-bit ADC digital sampling thresholds (which are fixed within the front end). When the gain is set too high (increased magnitude of real analog voltage samples), the sampled input signal falls disproportionally into the outer sampled bins which results in a non-ideal inverted sampling distribution.

Alternatively, if the commanded gain is too low the sampling shifts to the (lower voltage) inner two bins of the 2-bit sampling and results in a peaked sampling distribution. The optimal configuration is when the gain is commanded to a level which results in a near-ideal Normal (Gaussian) sampling distribution over the 4 digital sampled bins.

As the sampling distribution deviates from the Normal (Gaussian) shape, a small and gradual degradation in the downstream processed retrieved signal power levels arises [6]. It is important to note that GNSS signals when sampled off-air are typically at levels well below the input noise floor and are subsequently detected using a coherent (spread spectrum) processing technique in the digital signal processor such that the sampling distribution in a GNSS receiver is driven mostly by the input noise level [7].

It is convenient to define a single metric to quantify the digital sampling distribution. We have chosen to do this in a parameter called the Bin Ratio (BR), which is defined as,

$$BR = \frac{b_2 + b_3}{b_1 + b_4} \tag{18}$$

where, b_1, b_2, b_3, b_4 are, respectively, the number of counts accumulated into each of the four digital sampling bins, -3, -1, +1 and +3 respectively over a short time interval that in the case of the CYGNSS receivers is 1 second.

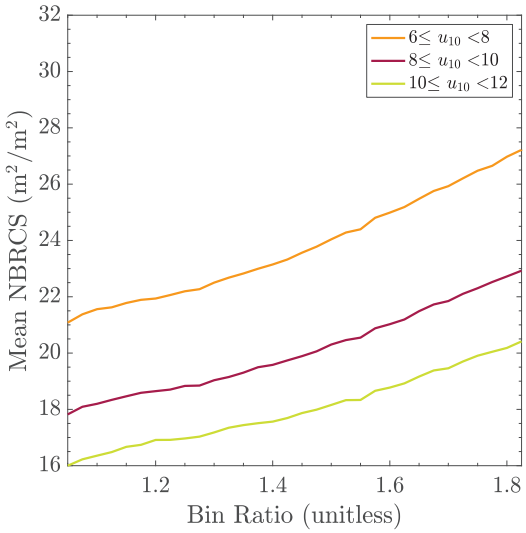

Fig. 2. Mean NBRCS estimates vs science channel bin ratio for three ranges of ocean conditions without digital sampling correction (ref. ECMWF).

B. Uncorrected NBRCS Dependence on Bin Ratio

In the idealized scenario of no calibration errors or uncertainties, NBRCS estimates should be independent of all instrument quantities with no correlation to bin ratios. Figure 2 demonstrates the observed, uncorrected, dependence of the NBRCS on Bin Ratio and wind speed.

C. Bin Ratio Correction Design

The Bin Ratio corrections contained in v3.1 included a noise only correction to the nadir channels and a signal counts based correction to the zenith channels, see [5]. However, this caused a degradation in performance to some Level 2 applications (notably Soil Moisture retrievals and ocean high wind sensitivity). After additional analysis of the correction mechanism, it is believed that this was due to the initial noise only correction neglecting the BR impact on other Level 0 count values in the L1a calibration; specifically the black body noise reference counts and the nadir signal counts (which includes the total counts minus the noise counts). Therefore the BR correction was redesigned with an additional correction to the black body counts and a new correction applied to the DDM signal counts.

The Zenith BR correction was left unchanged as that correction was applied and optimized on the total zenith signal counts which is the only observable available. Starting from the fundamental L1a calibration equation contained in the CYGNSS Level 1a ATBD Equation,

$$P_g = \frac{(C - CN)(P_B + P_r)}{C_B} \tag{19}$$

The baseline reference bin ratio correction is based on a theoretically modeled correction ("ref") and an (optional) empirical correction scaling factor (S_n), to give us the applied empirically corrected bin ratio correction factor ("emp"), expressed as,

$$\Gamma_{emp}(BR) = 1 - S_n \cdot \left(1 - \Gamma_{ref}(BR)\right) \tag{20}$$

The initial (v3.1) BR correction included this single correction applied to the estimated noise in the observation (C_N, DDM noise) term only,

$$C_{N,corr}(BR) = C_N(BR)\Gamma_{emp}(BR) \tag{21}$$

The new (v3.2) nadir BR correction includes corrections to both the signal counts (the total counts C minus the noise counts C_N) as well as the black body counts (C_B). The form of the black body counts correction is applied in the same manner as the previous versions noise correction, but with an empirical scale factor of 1.0 (i.e. the empirical correction is identical to the theoretical correction), expressed as,

$$C_{B,corr}(BR) = C_B(BR)\Gamma_{emp}(BR) \tag{22}$$

The v3.2 bin ratio correction also requires a correction to the received signal counts ($C - C_N$), which necessitates a re-arranging of the theoretical correction curve to enable its application to the received signal (in contrast to received noise, which the theoretical correction curve was generated assuming). The resulting positive signal correction can be expressed as,

$$\Lambda_{ref}(BR) = \Gamma_{ref}(BR) + 2 \cdot \left(1 - \Gamma_{ref}(BR)\right) \tag{23}$$

This reference correction can be scaled empirically as follows,

$$\Lambda_{emp}(BR) = 1 - S_n \left(1 - \Lambda_{ref}(BR)\right) \tag{24}$$

The corrected signal counts can then be expressed as,

$$C_{S,corr}(BR) = (C - CN)_{corr}(BR) = (C - CN)(BR)\Lambda_{emp}(BR) \tag{25}$$

Based on the performed empirical analyses of the signal correction, the optimal scale factor (S_n) was determined to be 1.0 (again, resulting in the empirical correction being equal to the and theoretical correction). The resulting Level 1a calibration equations are (with BR dependence terms removed to simplify),

$$P_g^{v3.1} = \frac{\left(C - C_{N,corr}\right)(P_B - P_r)}{C_B} \tag{26}$$

$$P_g^{v3.2} = \frac{C_{S,corr}(P_B - P_r)}{C_{B,corr}} \tag{27}$$

Both versions, v3.1 and v3.2, of the correction applied to C_N and (C - C_N) respectively are depicted in Figure 3. As the empirically derived scale factors for both of these corrections (S_n) are 1.0, these curves represent the theoretical bin ratio corrections (Γ_{ref} and Λ_{ref}).

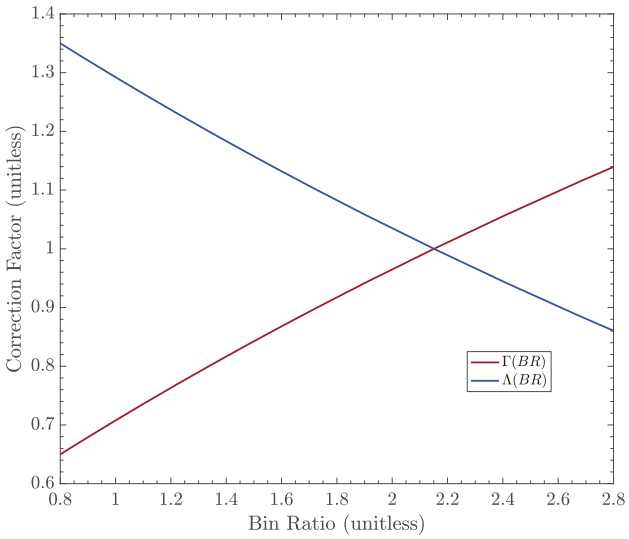

Fig. 3. Theoretical reference corrections used to account for digital sampling distortions in v3.1 and v3.2 of CYGNSS's Level-1 data releases

D. NBRCS vs Bin Ratio Dependence After New Correction

After the above v3.2 BR corrections were applied to both the black body load counts and the signal counts we were able to achieve consistently (flat) behavior across NBRCS as a function of BR and wind speed as shown in Figure 4. The resulting "flatness" of the corrected NBRCS vs BR performance amounts to an RMSD of 1.04 (linear) NBRCS over the range of BR containing 80% of the observations (lower and upper 10% of data is excluded from assessments given that observed trends can be heavily influenced by per-bin sparsity of data).

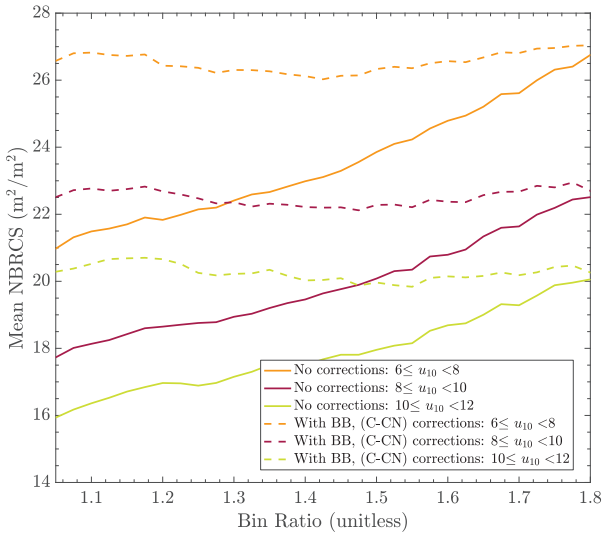

Fig. 4. Mean NBRCS estimates vs science channel bin ratio for three ocean wind speed conditions (ref. ECMWF) with digital sampling correction.

E. Bin Ratio Based Corrections Application To Zenith Channel Observables

The CYGNSS zenith observations consist of integrated signal plus noise counts only, without a reference noise floor. This prohibits the application of the nadir noise floor correction to the zenith channel observations. Note that a decrease in the noise floor in the nadir calibration is equivalent to an opposite adjustment to the total signal plus noise counts. The estimated power on the CyGNSS zenith antennas is used in the L1a calibration estimation of the Effective Isotropic Radiated Power (EIRP) during the conversion of signal power from Watts to a Normalized Bistatic Radar Cross Section (NBRCS). The observed zenith signal plus noise counts need to be corrected directly before a real-time EIRP estimate is formed [3, 8].

Like the nadir digital sampling correction, the zenith correction can also be optimized using empirical tuning factor(s) to ensure consistency of the EIRP estimation as a function of natural bin ratio fluctuations. Due largely to the spread of zenith bin ratio PDFs with means under that associated with an ideal Gaussian distribution, applying a single correction across all zenith observations was not possible and individual per-observatory corrections are required.

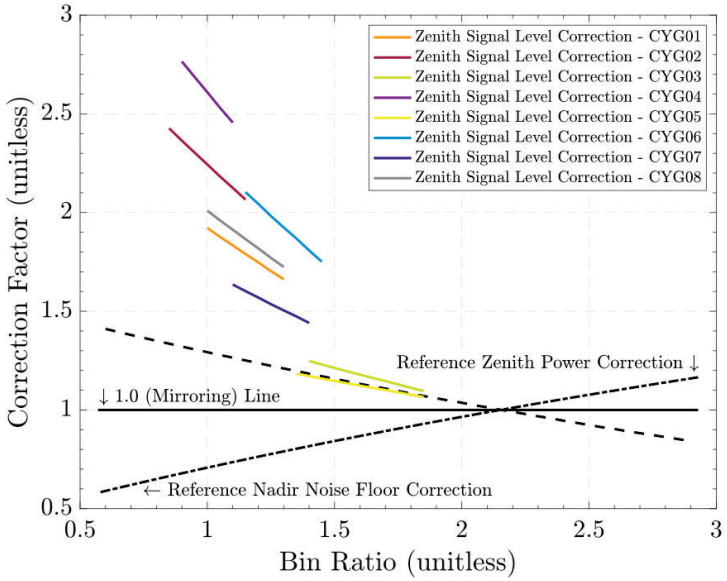

Fig. 5. CYGNSS FM specific zenith digital correction functions. Reference nadir correction is flipped around the 1.0 axis to accommodate the opposite signal plus noise counts correction. Scale factors are derived and applied to each FM individually. Corrections are shown for each FM over the 5%-95% range of observations where they are applied. This clearly demonstrates the deviation from the reference correction as the BR distribution shifts downward..

The per-FM zenith digital correction functions are shown in Figure 5. To better illustrate the need for an increased empirical correction factor as the mean BR of the distributions decreases, the per-FM corrections are shown only between their 5% and 95% bin ratio limits, to better illustrate the correction values where the on-orbit observations occur for each CYGNSS FM. As a given zenith bin ratio distribution approaches that of an ideal Gaussian distribution, only modest empirical adjustments are needed. For example see the CYG05 correction in Figure 5. In contrast, as the bin ratio distribution diverges from this ideal reference PDF, a need for significantly increasing the correction 'weights' at a given bin ratio is evident. An example of this is CYG04 which requires a much larger empirical scale factor.

The zenith signal digital corrections are evaluated with respect to the consistency of EIRP estimation across BR by each CYGNSS FM. An example of the before and after correction EIRP estimation across BR for CYGNSS FM 3 is shown in Figure 6. Before the digital sampling correction is applied there is a clear positive linear trend in the EIRP over a large range of BR (the bin ratio limits over which 95% of data occurs for a given FM). After the correction is applied the EIRP estimation is significantly more consistent (i.e. flatter) over the same BR range, reducing the maximum EIRP slopes by ~92%. The pre-correction and post-correction estimated EIRP root-mean-square-difference (RMSD) presented on a per-FM basis are listed in Table 3.

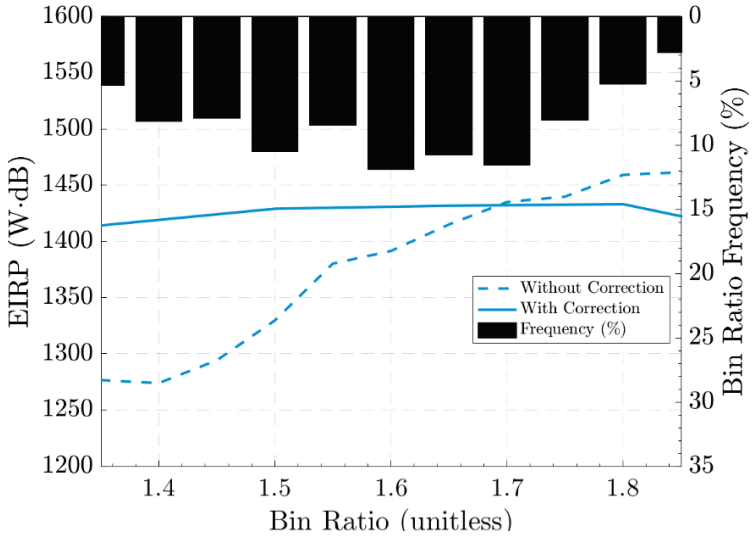

Fig. 6. Example zenith mean EIRP estimation over the BR range containing 95% of zenith observations for CYGNSS FM5. The pre-correction estimates (dotted line) clearly show a positive trend with BR that is largely mitigated with the digital sampling correction (solid line).

TABLE 2

SUMMARY OF CYGNSS ZENITH CHANNEL BIN RATIO DISTRIBUTIONS AND EIRP PRE-CORRECTION AND POST-CORRECTION PERFORMANCE

Parameter	FM 1	FM 2	FM 3	FM 4	FM 5	FM 6	FM 7	FM 8
Empirical Scale Factor, Y(FM)	3.15	4.25	1.35	5.5	0.93	4.4	2.4	3.45
Zenith BR Mean	1.17	0.99	1.64	1.01	1.64	1.35	1.25	1.16
EIRP RMSD, Uncorrected	113.97	123.88	96.76	101.19	72.69	130.3	101.17	102.85
EIRP RMSD, Corrected	23.91	28.99	20.91	16.18	22.83	23.4	24.21	19.57

REFERENCES

[1] Gleason, S., Ruf, C., Clarizia, M.P., O'Brien, A., Calibration and Unwrapping of the Normalized Scattering Cross Section for the Cyclone Global Navigation Satellite System (CYGNSS), IEEE Transactions on Geoscience and Remote Sensing, Vol. 54, No. 5, May 2016.

[2] C. E. Powell, C. S. Ruf and A. Russel, "An Improved Blackbody Calibration Cadence for CYGNSS," in IEEE Transactions on Geoscience and Remote Sensing, vol. 60, pp. 1-7, 2022, Art no. 1002407, doi: 10.1109/TGRS.2022.3165001.

[3] CYGNSS Science Team, CYGNSS Level 1b DDM Algorithm Theoretical Basis Document, 2017.

[4] Jansen, M.A., Ruf, C.S. and S.J. Keihm (1995), TOPEX/Poseidon Mircorwave Radiometer (TMR): II. Antenna Pattern Correction and Brightness Temperature Algorithm, IEEE Trans. Geosci. Remote Sens., Vol. 33, No. 1, pp. 138-146, January 1995.

[5] S. Gleason, M. Al-Khaldi, C. Ruf, D. McKague, T. Wang and A. Russel," Characterizing and Mitigating Digital Sampling Effects on the CYGNSS Level 1 Calibration," IEEE Transactions on Geoscience and Remote Sensing, (Accepted) October 2021.

[6] F.T. Ulaby and D.G. Long, Microwave Radar and Radiometric Remote Sensing; University Michigan Press: Ann Arbor, MI, USA, 2014.

[7] P. Misra and P. Enge, Global Positioning System: Signals, Measurements, and Performance. Ganga Jamuna Press, 2001. ISBN 0-9709544-0-9.

[8] T. Wang et al., ``Dynamic Calibration of GPS Effective Isotropic Radiated Power for GNSS-Reflectometry Earth Remote Sensing," IEEE Trans. Geosci. Remote. Sens., doi: 10.1109/TGRS.2021.3070238.